View metadata, citation and similar papers at core.ac.uk
brought to you by CORE
provided by Online Publishing @ NISCAIR

Indian Journal of Pure & Applied Physics
Vol. 56, September 2018, pp. 708-716

Microstructural and optical properties of La-doped ZnO thin films deposited by spin coating on quartz glass

Özlem Ertek Güldalı & İbrahim Okur*
Department of Physics, Sakarya University, 54187, Sakarya, Turkey

In this work, we have produced pure and composite zinc oxide-lanthanum oxide thin films. In the process we have started with a pure ZnO thin films and ended up with several lanthanum oxide phases containing thin films (La_2O_3, $La(OH)_3$ and LaOOH) by introducing La in various levels of concentrations, ranging from 0% to 100%. We have managed to attain crystal phases in all doping concentrations. All the produced thin films have been crystallized at the annealing temperatures of 1000 °C for duration of 6 h. The X-ray diffraction (XRD) patterns have been taken to see the formation of crystal phases of all pure and composite ZnO-lanthanum oxide thin films. XRD results gave insight that the various crystal phases related to ZnO and lanthanum oxide laid together within the thin film matrices, which have been produced in different doping concentrations. The scanning electron microscopy (SEM) micrographs and UV-Vis absorption studies have also been performed to elucidate the composed film structures, together with some optical parameters evaluation such as refractive index and dielectric constant.

Keywords: La-doped ZnO thin films, Spin coating, Microstructure, Structural and optical properties

1 Introduction

Metal oxide thin films are remarkable materials owing to their characteristic properties, one of which is a zinc oxide (ZnO). ZnO is a semiconductor material with a wide direct bandgap of 3.37 eV and high exciton binding energy of 60 meV at room temperature[1,2]. ZnO has a stable wurtzite structure with the lattice spacings[3] of a = 0.325 nm and c=0.521 nm. Zinc oxide nanostructures are of importance for novel size dependent applications in semiconductor and optoelectronic technologies with unique electrical and catalytic properties, high luminescence yield and low price[4,5]. Owing to their unique properties ZnO thin films can be used as field effect transistors, photovoltaic devices, energy efficient windows, ultraviolet (UV) photodetector, light emitting diodes (LEDs), varistors, liquid crystal displays, solar cells, chemical/gas sensors, antimicrobial staff, as well as feeding agents[6-9].

ZnO thin films can be prepared by various dry and wet chemical/deposition processes including; metal organic chemical vapor deposition (MOCVD), chemical vapor deposition (CVD), pulsed laser deposition (PLD), molecular beam epitaxy (MBE), magnetron sputtering, electrochemical deposition, spray pyrolysis and sol gel method[10,11]. Among these, sol-gel method has become a famous tool to make new kind of thin films and combining this with the spin coating method provides excellent film qualities. The spin coating method is very easy to implement and the cheaper than the others. With this technique some tens of cm^2 film areas can be produced on both the crystalline and amorphous surfaces. The crystalline quality of the film can be improved by the conventional annealing processes[12,13].

Over the past few years, rare earth elements (such as La, Dy, Nd, Ce, Sm, Gd, etc) doped nanocrystals have attracted considerable attention since they can greatly enhance the optical and electrical properties of the main structure. Rare earth elements are known to be laser active when they are integrated/doped into the various amorphous and crystalline structure to get especially IR radiation that can be used in various applications[13-16]. They can also change the electrical and structural properties of the thin films by choosing the appropriate dopant type and doping concentrations[17-19].

In this paper, we have outlined the experimental results together with some evaluations related to the La incorporated ZnO thin films produced in different percentages and presented their optical, structural and electrical properties. The films have been produced by spin coating method. The samples annealed at 1000 °C for six hours have been investigated by using XRD,

*Corresponding author (E-mail: iokur@sakarya.edu.tr)

SEM, and UV-Vis absorption spectroscopy. We have also given some optical constants of pure and La incorporated ZnO thin films, such as the band gap, refractive index, extinction coefficient, dielectric constant and dispersion parameters.

2 Experimental

All the chemical used in this work were of analytical grade purchased from Sigma Aldrich. Pure and La incorporated ZnO thin films have been deposited onto the quartz substrates by using the spin coater. For the pure ZnO thin films, zinc precursor solution was prepared by dissolving zinc acetate dehydrate ($C_4H_{10}O_6Zn$) in methoxyethanol ($C_3H_8O_2$) together with some pure water in proper ratio to obtain 0.5 M concentration. In this process monoethanolamine was used as a complexing agent. For the La incorporated zinc oxide and pure lanthanum oxide films, lanthanum acetate ($La(CH_3COO)_2.H_2O$) has been used with methoxyethanol ($C_3H_8O_2$) and sol has been obtained with 0.5 M concentration. These two solutions have been used to attain the desired mixing concentrations. For example, for 5% La doping, 5:95 ratio has been used to obtain the La:ZnO incorporated films. We have chosen the lanthanum level of concentrations of 2, 5, 10, 20, 50, 80 and 100%. All solutions were mixed at 70 °C/1h using magnetic stirrer (Wisestir, MSH-20A) at atmospheric pressure. The films were then spin coated on quartz glasses at the speed of 500 rpm and undergone ten layers of deposition. Each layer was dried at 250 °C for 10 min to remove the residual parts from the films. Having completed the ten layers of coatings, the thin film coated samples were annealed at 1000 ^{o}C for six hours at a furnace (Nabertherm B170) to reach the crystal phase (Fig. 1). This process was repeated for the pure ZnO, lanthanum oxide and the mixture of ZnO/lanthanum oxide thin films and all the samples have been analyzed by means of the XRD, SEM and UV-Vis spectrometry.

The XRD pattern of the produced thin films (ZnO, lanthanum oxide and the mixture of the two in proper ratios) has been recorded by means of an XRD diffractometer (Rigaku D/Max 2200PC) using CuK_{α} band (λ= 0.154 nm). The SEM micrographs of all the samples have been taken using an SEM (JEOL 6060LV) spectrometer. The UV-Vis spectra of ZnO and La incorporated ZnO thin films have been obtained by using Agilent 8453 UV-Vis spectrometer.

3 Evaluation of Optical Constants and Dielectric Characterization

The transmittance of the thin films can be calculated by using the formula:

$$T = 10^{-A} \quad \dots (1)$$

where A is the absorbance which is generally taken during the absorption experiments. If one evaluates the transmittance from the Eq. (1) then it is likely to reach the reflectance (R) as well with the help of the conservation of the energy which yields:

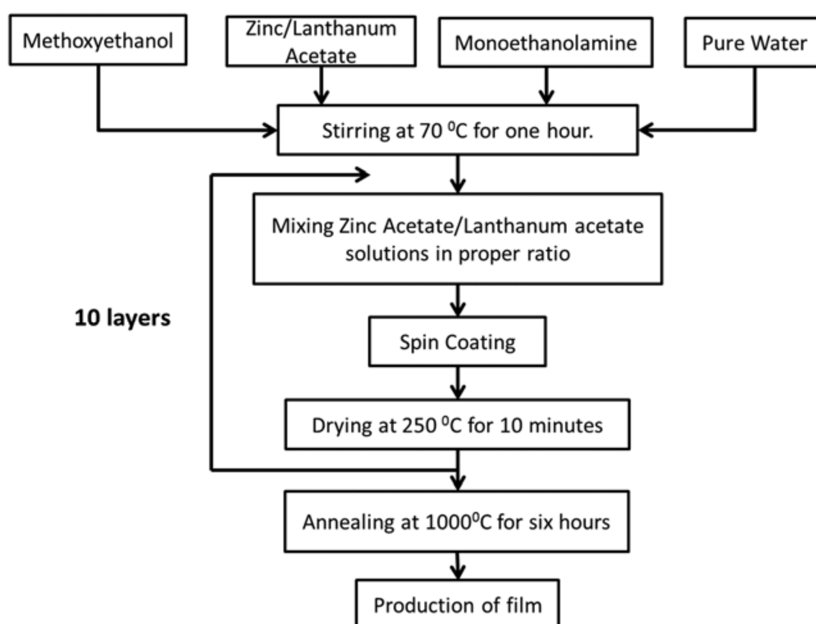

Fig. 1 — Flow diagram of the ZnO and lanthanum oxide composite thin film production process.

$$A + T + R = 1 \qquad \ldots (2)$$

The optical absorption coefficient (α) is calculated from the transmittance using the following equation[20]:

$$\alpha = -\frac{\ln(T)}{d} \qquad \ldots (3)$$

where T is the transmittance and d is the thickness of the thin film. In general the equation used to determine the band gap energy (E_g) values of the thin film (for the direct bandgap thin films) is as follows[21]:

$$\alpha = \frac{K\sqrt{(h\nu - E_g)}}{h\nu} \qquad \ldots (4)$$

where $h\nu$ is the photon energy and K is an energy-independent constant. The refractive index of the thin films can be found employing the formula[22,23]:

$$n = \left(\frac{1+R}{1-R}\right) + \sqrt{\frac{4R}{(1-R)^2} + k^2} \qquad \ldots (5)$$

in which the optical extinction coefficient is defined to be:

$$k = \frac{\alpha\lambda}{4\pi} \qquad \ldots (6)$$

where λ is the wavelength of incident light beam. The complex refractive index $n^* = n + ik$ and the dielectric function $\varepsilon^*(w) = \varepsilon'(w) + i\varepsilon''(w)$ characterize the optical properties of the thin solid films. The real and imaginary parts of the complex dielectric constants are evaluated by using the following formulas[23]:

$$\varepsilon'(w) = n^2(w) - k^2(w) \qquad \ldots (7)$$

$$\varepsilon''(w) = 2\,n(w)\,k(w) \qquad \ldots (8)$$

4 Results and Discussion

4.1 XRD pattern

For all the doping concentration levels it has been found that all the films were crystallized when annealed at 1000 °C. Doping the element lanthanum to the ZnO structure has shown us that the various lanthanum oxide crystal phases have been formed within the matrix, i.e., La_2O_3 (lanthanum oxide), $La(OH)_3$ (lanthanum hydroxide), LaOOH (lanthanum oxohydroxide) and $La_2Si_2O_7$ (lanthanum disilicate). In all of the doped samples, ZnO classical peaks exhibited themselves in the XRD pattern (Fig. 2(a-g)) up to 80% lanthanum added case (Fig. 2(g)). This means that ZnO nanocrystal phase remains inside the thin film structure together with the lanthanum oxide phases. If one carefully examines the XRD results it can be concluded that the various lanthanum oxide phases exhibit themselves and the XRD intensity values of these crystal phases increase when the doping level is increased. During the doping process it is understood from the XRD patterns that these lanthanum oxide crystal phases are difficult to analyze due to the fact that a lot of phases are formed within the structure and their classical XRD peaks are very close to each other. In another work performed in our group using the other lanthanide element (Dy) this was not the case, only one crystal phase has been obtained[24]. This gives us the clue that the lanthanum is special in that when it is used as dopant/incorporating agent for the zinc oxide thin film structures.

4.2 SEM micrographs

SEM images show rather porous films having major defects, such as cracks, exfoliations and possible discontinuous areas. From these images it has been perceived that in general the grain sizes and shapes changes completely by changing the La level of concentration. For example, nanorod like structure starts gradually to disappear after 10% La doped ZnO thin films (Fig. 3(a-c)), reaching to a spherical/rocky/cluster-like structures (Fig. 3(d-h)). When these photographs carefully examined it has been concluded that the nanorod structures has the diameter starting at 500 nm for pure ZnO structure, gradually decreasing down to 100 nm up to 10% La doped thin films. The radii of the produced nanorods start to increase after 20% La added case up to 300 nm. After 50% La incorporated level of concentration the radii start again to decrease down to 80 nm. A porous thin film structure forms especially at and after 20% lanthanum incorporated samples (Fig. 3(e)). The cracks, resulting from the high temperature annealing process, seem to disappear when 50% and higher ranges of lanthanum adding levels reached and snowflakes like structure is reached (Fig. 3(h)), which we suggest that the reason for that is likely to be the sintering effects in progress. When the nanorod structures in these SEM photographs is investigated it is found that the nanorods form at the lower La incorporating level of concentrations up to 10% and the length of these rods are calculated to be 100 microns with a radius of 1-2 microns. After 10% La adding concentrations these rods were disappeared

and homogenous structures were reached, either in leaf-like or snowflake-like in shape.

4.3 UV-Vis spectra

The spectra for the samples annealed at 1000 °C for six hours have been depicted in Fig. 4. From the spectra it has been perceived that the main absorption peak situated at 193 nm for pure ZnO thin film conserves the position though small amount of wavelength shift occurs (redshift), which might be attributed to the fact that the diameter of the nanoparticles decreases by increasing the La doping

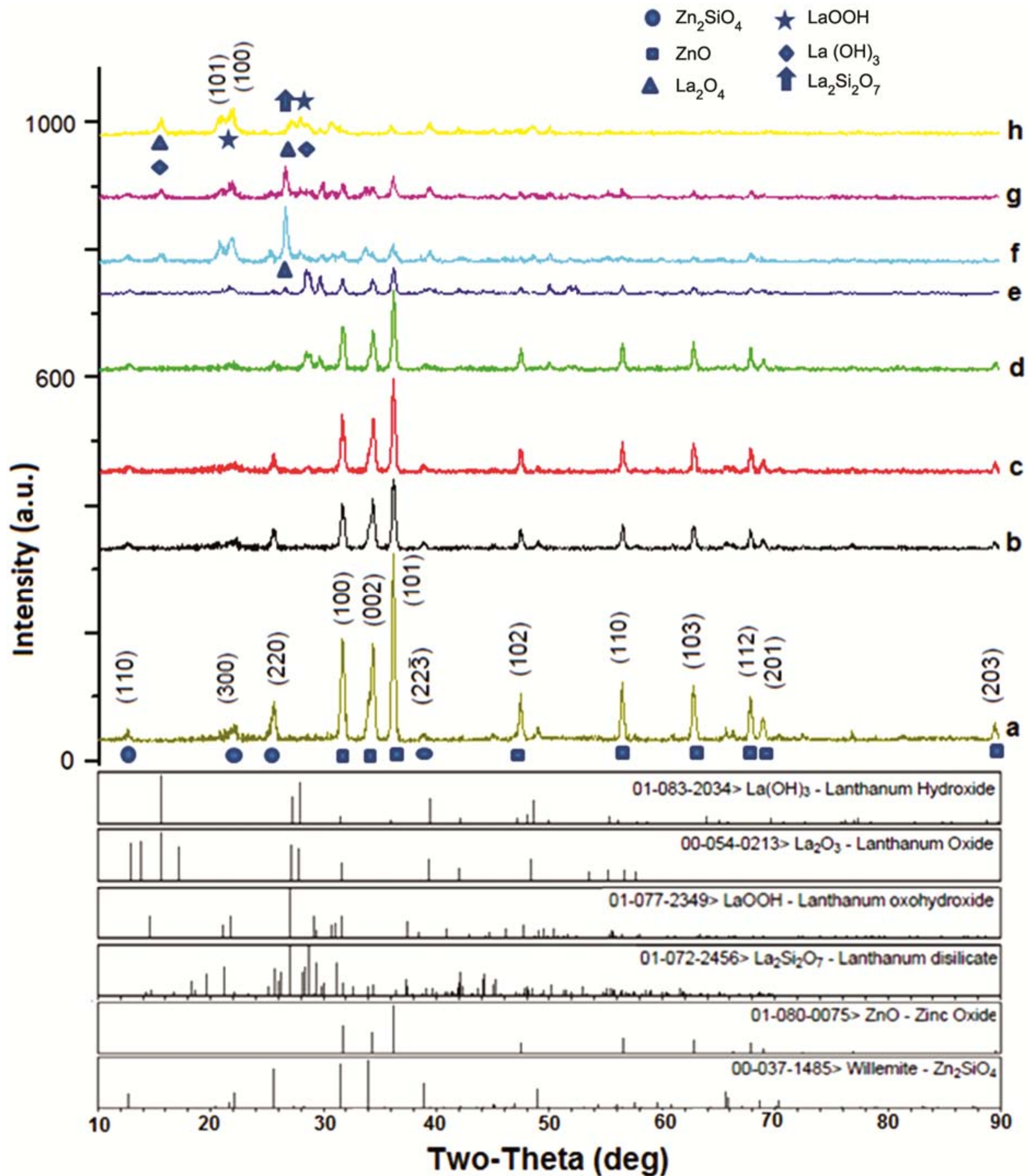

Fig. 2 — XRD patterns of the thin films annealed at 1000 °C for (a) undoped ZnO, (b) 2%, (c) 5%,(d) 10%, (e) 20%, (f) 50%, (g) 80% and (h) 100% lanthanum incorporated ZnO thin films on quartz substrates. Some diffraction peaks related to zinc oxide and lanthanum oxides are denoted inset the figure.

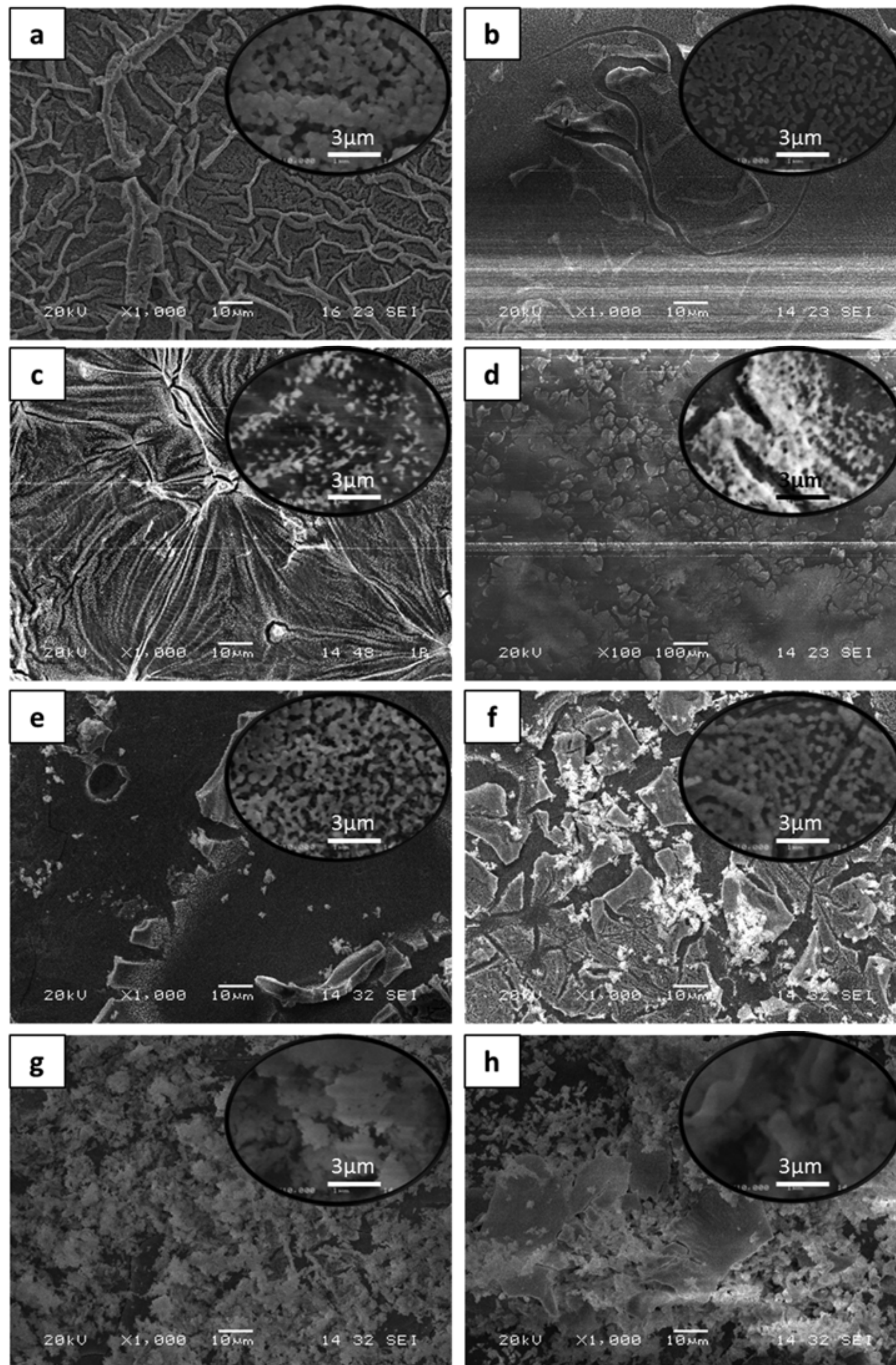

Fig. 3 — SEM images of the pure and lanthanum incorporated zinc oxide thin films, (a) undoped (ZnO), (b) 2%, (c) 5%, (d) 10%, (e) 20%, (f) 50%, (g) 80% lanthanum added ZnO and (h) 100% lanthanum oxide, annealed at 1000 °C.

level. This peak is diminished when reached the pure lanthanum oxide thin films, i.e., 100% La doping case (Fig. 4 (h)). It should be noted here that the classical ZnO absorption bands situated at 370 nm is not the case in our samples since this band is obtained when the annealing temperature is chosen to be 600 °C and higher temperature annealing diminishes this band and creates the new one[6,12,25] at 193 nm.

4.4 Optical constants and dielectric characterization

Optical transmittance spectra of the pure and lanthanum doped ZnO thin films in various percentages have been depicted in the Fig. 5, using

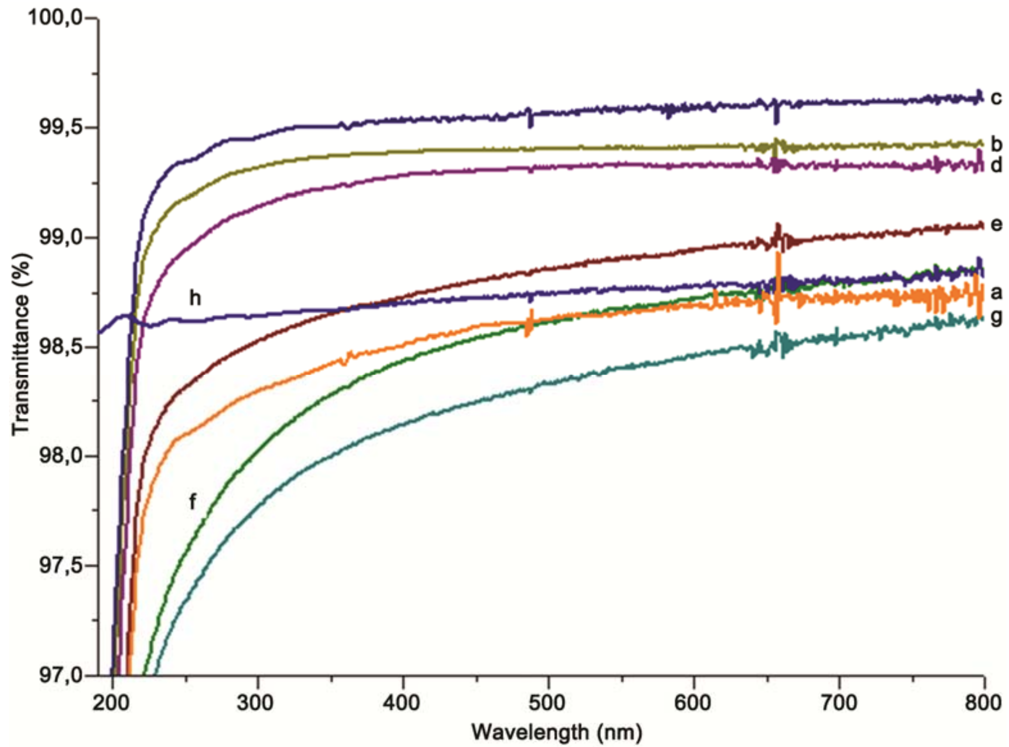

Fig. 4 — UV-Vis spectra of lanthanum incorporated zinc oxide thin films (190-260 nm wavelength interval is given in the figure), (a) undoped (ZnO), (b) 2%, (c) 5%, (d) 10%, (e) 20%, (f) 50%, (g) 80% lanthanum incorporated ZnO and (h) 100% lanthanum oxide films.

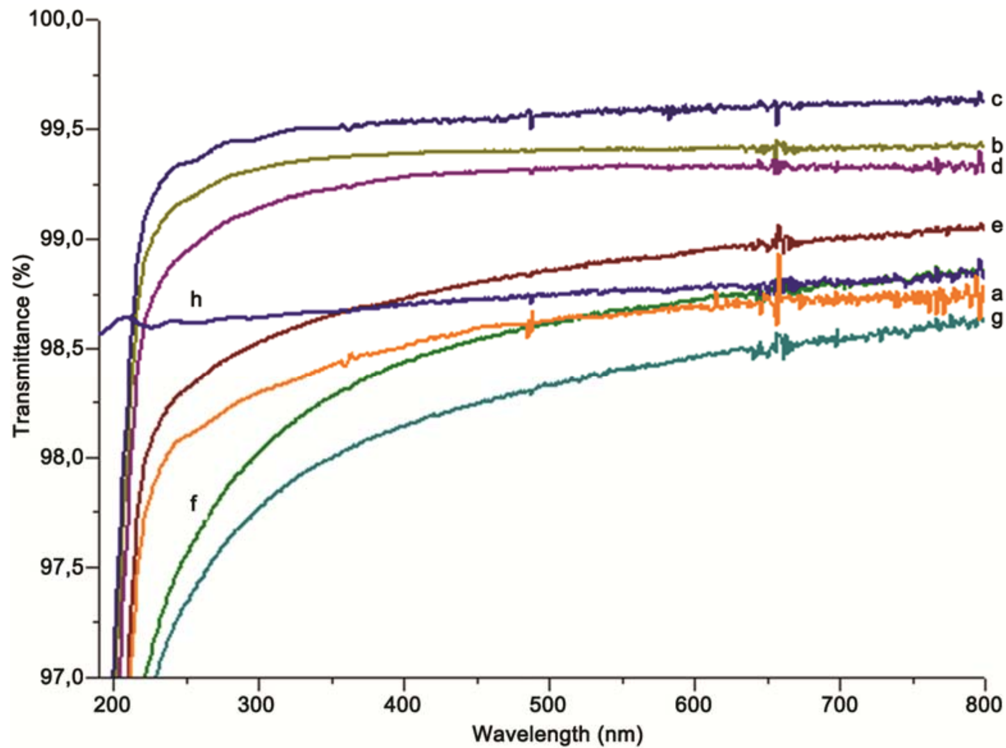

Fig. 5 — Optical transmittance spectra of lanthanum incorporated zinc oxide thin films (a) undoped (ZnO), (b) 2%, (c) 5%, (d) 10%, (e) 20%, (f) 50%, (g) 80% lanthanum added ZnO and (h) lanthanum oxide films.

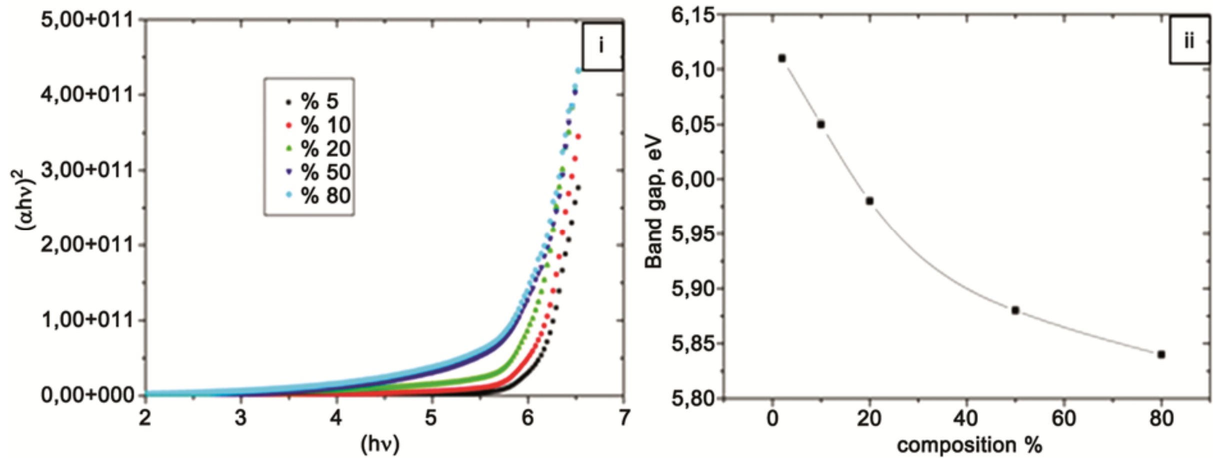

Fig. 6 — (a) Photon energy versus $(\alpha h\nu)^2$ for the films for various lanthanum level of concentrations and (b) the E_g values versus composition level.

the absorption spectra and Eq. (1). From the spectra it can easily be seen that the films have the higher transmittance values up to 99.5%, showing that the films produced are transparent especially in the near UV and visible region.

The E_g values for the films have been obtained from the plot of variation of $(\alpha h\nu)^2$ versus the photon energy in which the Eqs (3) and (4) were used in which the film thickness was 0.76 µm. The energy gap values were evaluated by the extrapolation of the graph to the energy axis (Fig. 6(a)). For the 100% lanthanum incorporated (pure La) case the thin film became metallic and we have not evaluated any E_g values for that film. It is surprisingly interesting that the energy gap values decreases down to the lower values by increasing the doping concentration, which can be thought that the films are getting more metallic (Fig. 6(b)). The decrease in E_g value seems to obey an exponential decay law, i.e., exp($-f\rho$) where ρ denotes the doping concentration and f is a constant. From the graph (Fig. 6(a) we have evaluated the constant f to be 4.7×10^{-4} mol^{-1}, which seems to be a dopant sensitive value.

The produced thin films' refractive index variation has been evaluated by using the Eq. (5) and we have obtained the dispersion curves (Fig. 7). As can be seen from the figure that the increase in the La level of concentration slightly increases the refractive index of the films.

As mentioned before, the total dielectric functions for the samples can be expressed by $\varepsilon^*(w) = \varepsilon'(w) + i\varepsilon''(w)$, where ε' is real and ε'' is the imaginary part of the function and $w = 2\pi f$ is the angular frequency of the

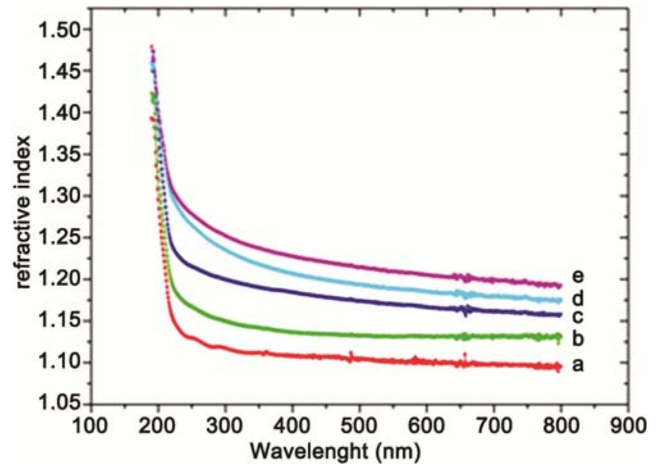

Fig. 7 — Refractive index versus wavelength for (a) 5%, (b) 10%, (c) 20%, (d) 50% and (e) 80% lanthanum contained zinc oxide thin films.

incident photon. These quantities can be easily derived from the analysis of the quantities of refractive index and decay functions to be $\varepsilon'(w) = n^2(w) - k^2(w)$ and $\varepsilon''(w) = 2n(w)k(w)$. From Fig. 8 one can conclude that the real dielectric constant initially increases very slowly by increasing the photon frequency and then the increase has a sudden jump to higher values after the frequency of 1.3×10^{15} Hz for all the samples.

For both lower and higher frequency values the dielectric constant increases by raising the lanthanum level of concentrations. If one considers that the contribution to the polarizability in the higher frequency region comes only from the electronic part, one may conclude that the increase in lanthanum doping level clearly raises the electronic polarizability to higher values. In addition to that, in the lower

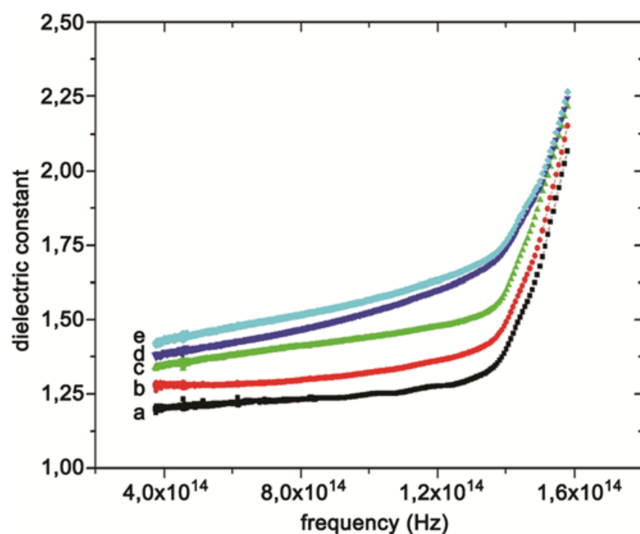

Fig. 8 — The variation of dielectric constant versus photon frequency for (a) 5%, (b) 10%, (c) 20%, (d) 50% and (e) 80% lanthanum added zinc oxide thin films.

frequencies smaller than these frequency intervals the polarizability is always decreased by increasing the frequency. However, it can be concluded that the unique reason for that increase in the frequency interval might be attributed to the dielectric resonance caused by the electrons hopping from the valence to the conduction band. In the higher frequency region one can imagine that there exists a resonance which is not clearly seen but starting to grow. The reason for that the resonance is not completed can be interpreted that this resonance needs lower wavelength photons for all samples. One can easily estimate that the resonance will shift to higher frequencies by increasing the lanthanum doping level. As mentioned above, this can be explained by using the band gap of the lower level of lanthanum incorporated zinc oxide sample.

5 Conclusions

In this study lanthanum doped ZnO thin films in various concentrations were fabricated on quartz glasses using the spin coating method and the optical properties of these samples were investigated using XRD, SEM and UV-Vis absorption spectroscopy. Some optical constants and dielectric characterization of the samples were also been evaluated. It has been found that for all lanthanum doping concentrations, ranging from 2% to100%, crystal structures were obtained. From the XRD patterns it has been found that the thin films inhibited both the ZnO and the various lanthanum oxide crystal structures (La_2O_3, $La(OH)_3$, LaOOH and $La_2Si_2O_7$) together within the film matrices as their diffraction peaks presented in the spectra and the doping concentrations reflected themselves exactly in the same peak heights, therefore the presence of one have not any impact of suppressing the other's intensity.

From the SEM images it has been found that the grain sizes and shapes changes by changing the lanthanum doping level. Nanorod like structure disappears after 10% La doped ZnO thin films ending up with a spherical/rocky/cluster-like structures. The nanorod structures has the diameter of 500 nm for pure ZnO structure, decreasing down to 100 nm up to 10% La doped thin films and then starts to increase after 20% La doping cases up to 300 nm (for 50% La doping case). For higher doping concentrations (i.e., 80 and 100%) the radii start to decrease down to a value of 80 nm. A porous thin film structures are obtained for the 20% and higher level lanthanum doped thin films.

The absorption spectra for the samples annealed at 1000 °C for six hours have shown a peak at 193 nm for pure ZnO thin film and this peak stays consistent up to higher level lanthanum doping cases with a small amount of wavelength shift and it diminishes when reached the pure lanthanum oxide thin films. The transmittance spectra of the films show that the all films have the higher transmittance values up to 99.5%.

It has been found that the energy gap values stay around 6.14 eV to 5.84 eV, so that the increasing the doping level decreases the energy gap values, obeying an exponential decay law. The increase in the doping concentration of the lanthanum increases generally slightly the refractive index of the films. From the evaluation of the dielectric constant it has been found that it increases by raising the lanthanum doping concentrations for both lower and higher frequency values and the increase in lanthanum doping level clearly raises the electronic polarizability to the higher values.

Acknowledgement

Authors would like to thank to Sakarya University and TUBITAK (Project Number: 1649B031305861) for the financial support and Fuat Kayış for careful work on taking the SEM and XRD patterns.

References

1 Deng S H, Duan M Y, Xu M & He L, *Physica B*, 406 (2011) 2314.
2 Narinder K, Sanjeev K S & Deuk Y K, *Curr Appl Phys*, 16 (2016) 231.

3 Kaya B A, ErtekGüldalı O, Eker N & Okur I, *Mater Sci Appl*, 6 (2015) 40.
4 Wu T, Ni Y, Ma X & Hong J, *Mater Res Bullet*, 48 (2013) 4754.
5 Alfaro C M R, Hernandez-Como N, Mejia I, Ortega Zarzosa G, Martínez Castañón G A & Quevedo-Lopez M A, *Mater Lett*,133 (2014) 293.
6 Nalbant A, Ertek O & Okur I, *Mater Sci Eng B*, 178 (2013) 368.
7 AdirajIyer M, Ozaa G, Velumani S, Maldonadoa A, Romeroa J, de L Munoz M, Sridharanb M, Asomozaa R & Yi J, *Sens Actuators B*, 202 (2014) 1338.
8 Zhou H, Fang G J, Liu N & Zhao X Z, *Mater Sci Eng B*, 176 (2011) 740.
9 Shankar S, Teng X, Li G & Rhim J W, *Food Hydrocolloid*, 45 (2015) 264.
10 Lu H, Wang Y & Lin X, *Mater Lett*, 63 (2009) 2321.
11 Zhang S, Zhang W & Lu G, *Mater Lett*, 138 (2015) 262.
12 Nalbant A, Ertek O & Okur I, *Arab J Sci Eng*, 38 (2013) 1909.
13 Chen J T, Wang J, Zhang F, Zhang G A, Wu Z G & Yan P X, *J Cryst Growth*, 310 (2008) 2627.
14 Avram D, Gheorghe C, Rotaru C, Cojocaru B, Florea M, Parvulescu V & Tiseanu C, *J Alloys Compd*, 616 (2014) 535.
15 Korake P V, Dhabbe R S, Kadam A N, Gaikwad Y B & Garadkar K M, *J Photochem Photobiol B: Biol*, 130 (2014) 11.
16 Bünzli J C G, *Coord Chem Rev*, 293 (2015) 19.
17 Jia T, Wang W, Long F, Fu Z, Wang H & Zhang Q, *J Alloys Compd*, 484 (2009) 410.
18 Iwan S, Zhao J L, Tan S T, Bambang S, Hikam M, Fan H M & Sun X W, *Mater Sci Semicond Proc*, 30 (2015) 263.
19 El Hachimi A G, Zaari H, Benyoussef A, El Yadari M & El Kenz A, *J Rare Earths*, 32 (2014) 715.
20 Benouis C E, Benhaliliba M, Yakuphanoglu F, Tiburcio S A, Aida M S & Sanchez J A, *Synthetic Metal*, 161 (2011) 1509.
21 Shankar G, Joseph P S, Suvakin M Y & Sebastiyan A, *Opt Commun*, 295 (2013) 134.
22 Yakuphanoglu F, Cukurovali A & Yilmaz İ, *Opt Mater*, 27 (2005) 1363.
23 Yahia I S, Farag A A M, Cavas M & Yakuphanoglu F, *Superlattices Microstruct*, 53 (2013) 63.
24 Ertek O & Okur I, *Indian J Pure Appl Phys*, 54 (2016) 99.
25 Ertek O & Okur I, *Int J Thermophys*, 36 (2015) 1673.